Journal of
Marine Science
and Engineering

MDPI

*Article*

# Dynamic Inversion Model of the Mooring Force on a Floating Bollard of a Sea Lock

**Linjian Wu [1], Zhouyu Xiang [1,*], Dan Shu [2], Mingwei Liu [1,*], Jia Yang [1] and Minglong Li [3]**

[1] National Engineering Research Center for Inland Waterway Regulation, School of River and Ocean Engineering, Chongqing Jiaotong University, 66 Xuefu Road, Nan'an District, Chongqing 400074, China
[2] Chongqing Shipping Engineering Survey and Design Institute of the Yangtze River, Chongqing 400074, China
[3] Sichuan Communication Surveying and Design Institute CO., LTO, Sichuan 610000, China
* Correspondence: xzy@mails.cqjtu.edu.cn (Z.X.); 990000950717@cqjtu.edu.cn (M.L.)

**Abstract:** Sea locks that connect inland canals and rivers to the open sea are crucial links that ensure the efficient navigation of ships. Floating bollards (FBs) are significant components of sea locks, and they are affected by factors such as large ships, speed of entry, and irregular mooring lines coupled with corrosion by chloride salts from seawater intrusion from the environment. These factors aggravate damage to metal structures, which seriously threatens the safety of FBs. Overloading of FBs by mooring forces caused by the illegal use of FBs for the braking of large ships that enter locks at excessive speed is the main cause of structural damage and overload failure for FBs. Controlling the dynamic mooring force acting on the FB is an important prerequisite to ensure the safe passage of a ship through a lock. It is impossible to perform real-time monitoring of the magnitude and direction of the mooring force on an FB by installing load-measuring equipment on the mooring line. Therefore, in this study, the structure of an FB in a sea lock project was taken as an example, and the mathematical relationships between the strain in the load-sensitive area of the FB and the mooring force and the mooring angle were quantified. A dynamic inversion model of the ship mooring force on an FB was proposed. This model used real-time feedback from the strain signal in the load-sensitive region of the FB structure to obtain information about the mooring force. The accuracy of the model was verified by conducting tests with a physical model of the topside structure of the FB and comparing the predicted results with the test data. The research results can lay a theoretical foundation for real-time monitoring of the structural response of an FB under the action of mooring forces and promote the development of intelligent methods for the operation and maintenance of a sea lock, which have important scientific significance and engineering value.

**Keywords:** sea lock; floating bollards; bollard load calculation; mooring forces; dynamic mooring analysis; model test



**Citation:** Wu, L.; Xiang, Z.; Shu, D.; Liu, M.; Yang, J.; Li, M. Dynamic Inversion Model of the Mooring Force on a Floating Bollard of a Sea Lock. *J. Mar. Sci. Eng.* **2023**, *11*, 1374. https://doi.org/10.3390/jmse11071374

Academic Editor: Marko Perkovic

Received: 24 May 2023
Revised: 2 July 2023
Accepted: 3 July 2023
Published: 5 July 2023



## 1. Introduction

Problems with mooring safety in sea locks connecting inland canals and the open sea [1,2] are usually related to structural overload and damage to bollards directly caused by the mooring force or deterioration of the material properties of metal indirectly caused by corrosion related to environmental factors such as seawater intrusion [3–8]. Mooring systems are of vital importance for offshore floating facilities [9–12], and bollards are a key part of mooring systems at the sea lock, which are anchor points for mooring lines used to secure a vessel or ship [13]. They can generally be classified as fixed bollards and floating bollards (FBs) [14]. The former is often installed in the upper part of the harbor for ship mooring [15,16], and the latter is used in the lock to ensure the safe berthing of the ship during changes in the water level in the lock chamber [14]. The Miraflores locks that have been built on the Panama Canal [17,18] (see Figure 1a), the Qingnian lock of the Pinglu Canal under construction in China [19] (see Figure 1b), and other types of locks in estuaries are important navigable structures connecting inland canals and the open sea, and they are crucial links that ensure the efficient navigation of ships from rivers to the sea. As a significant component of a sea lock, the normal service of an FB is key to ensuring the safe operation and efficient navigation of a lock. However, large ships, excessive speeds of entry, irregular mooring, and other factors, including corrosion caused by chloride salts from the environment as a result of seawater intrusion, aggravate the damaging and destruction of metal structures and seriously threaten the service safety of FBs [20–25]. In addition, damage to the main structure of an FB induces deformation of the guide trough and blockage of the pulley, which leads to accidents such as pulling the ship into the water, damaging the hull, and causing casualties, resulting in very large economic losses and negative impacts on society.

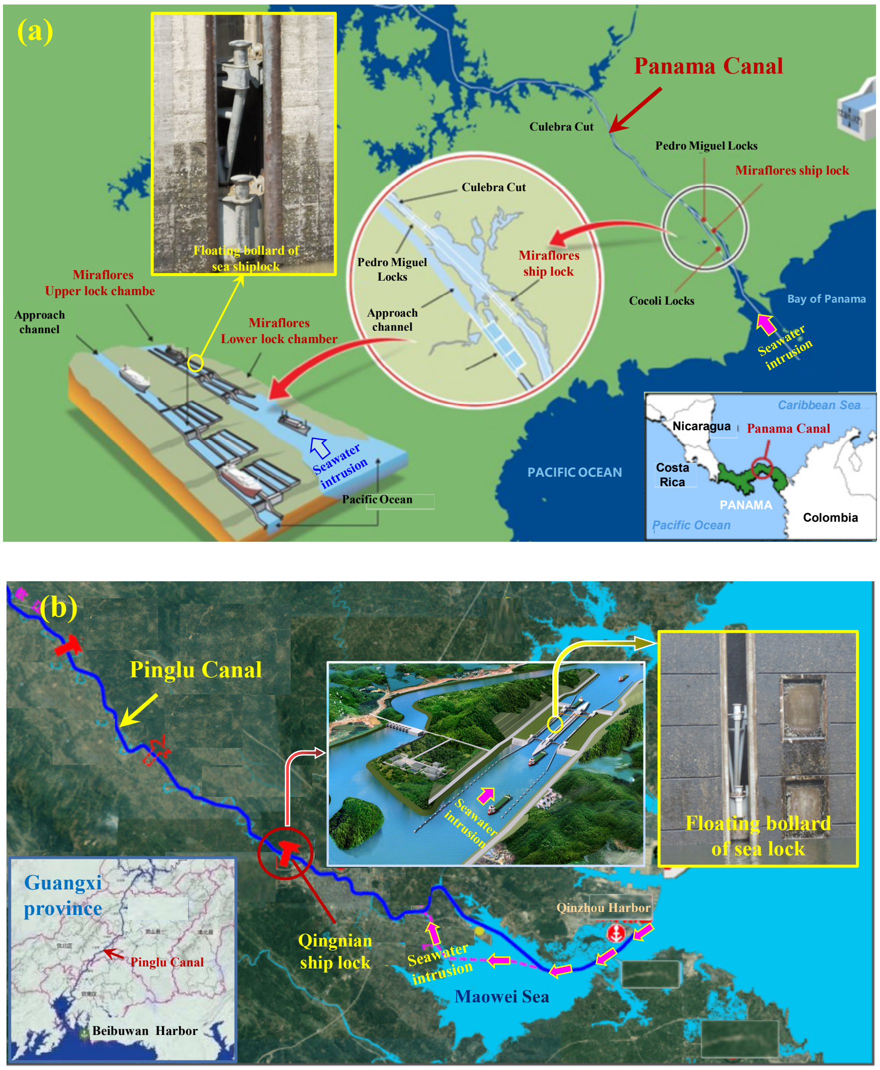


**Figure 1.** Typical sea locks: (**a**) the Miraflores ship lock of the Panama Canal [17,18]; (**b**) the Qingnian ship lock of the Pinglu Canal in China [19].

Information such as the magnitude and direction of the mooring force can directly reflect the operating state of the bollard (regardless of whether it is a fixed bollard or a floating bollard) and can serve as an important basis for the evaluation of safe mooring conditions for navigable ships [26–28]. Therefore, scholars at home and abroad have conducted relevant research on how to obtain the mooring force acting on a bollard [29–31]. A simplified linear static methodology for estimating the maximum tension of mooring lines and the compression of fenders for a ship berthed at a bollard on the structure of a port was proposed by De Carvalho et al. [29]. For fixed bollards, a real-time inversion method and a method of monitoring the standard mooring force based on multi-point strain information fusion was proposed by Wu et al. [32], which can satisfy the need for monitoring the mechanical safety of bollard structures under complex mooring conditions. Cho et al. [33] showed that the ultimate bearing capacity of a bollard under a mooring force could not be significantly improved by strengthening the bollard, and they suggested that the structural resistance of the bollard could be improved by enhancing the material properties and improving the casting process of the structure.

For a floating bollard, an overloaded mooring force caused by the illegal use of an FB for braking a large ship that enters a lock at excessive speed is the main cause of structural damage and overload failure for FBs [34,35]. The responses of the floating structure in different water depths and sea states were studied to clarify safe conditions for a float-over installation in shallow water [36]. Dynamic control of the mooring force acting on the FB is an important prerequisite to ensure the safe passage of the ship. The influence of the change in water level within the lock on the mooring force was studied, the relevant definitions and test methods used in the design criteria of the lock mooring facilities were discussed, and the traditional mooring force calculation criteria were revised [37]. The effect of the density difference on the force of the moored ship under density flow was investigated [38], and the research showed that, due to the difference in water flow density and the asymmetric arrangement of moored ships in the lock chamber, the mooring force of navigable ships exceeded the allowable mooring force of the FB. The mooring force of a ship is measured by cutting the mooring line and installing a tension sensor at the break; the allowable value of the mooring force on the FB can be used to evaluate the safety of the ship mooring, as proposed by [39]. Most of the mooring forces measured by previous researchers referred to the total tension in only one direction (longitudinal or transverse), and it was impossible to deeply analyze or study the nature of the force; thus, a new method for evaluation of the mooring condition was developed [40]. A new saddle-type tension sensor was designed to measure the tension of an FB [41], and dynamic monitoring of the safe operating state of the FB was realized. Qiao et al. [42] investigated the motion responses of the mooring lines of floating structures in a slack–taut process, the slack–taut alternating transformations were simulated, and the variation law of dynamic tension in mooring lines was analyzed. A new stress–strain constitutive model was proposed by Huang et al. [43] based on Schapery's theory and Owen's rheological theory, which can fully take into account the loading history and the time-dependent property of synthetic fiber ropes under cyclic loading. On this basis, an experimental system that can approximately simulate the practical working condition of mooring ropes was developed [44].

However, the mechanical characteristics of an FB cannot be reflected effectively by installing tension sensors and other load-measuring equipment on the mooring line. There is no supervision initiative for the navigable hub management unit, which cannot track and completely monitor the mooring state of all navigable ships in the lock chamber in real time for safety. A series of studies have been carried out on the mechanical characteristics of FB structures. Liu Mingwei et al., relying on the cylindrical FB structure in the lock of the Gezhouba Project in China, conducted a structural force analysis of FBs under different mooring forces and mooring angles based on the finite element numerical simulation method [45]. On this basis, a mechanical model for the load response of the FB was derived when the vertical mooring angle was positive [46], and the reliability of the model was verified by field test data for an FB in a lock in China [47].

In summary, as far as the FB of a sea lock is concerned, the conventional means of installing load-measuring equipment on the mooring line of a ship cannot obtain important data such as the mooring force and mooring angle of the FB in real time. Moreover, this passive measurement method heavily relies on the active cooperation of the passing ship, which makes it difficult for the navigation hub management unit to actively perceive the operational state of the FB. Thus, there is an urgent need to develop a method for determining the mooring force with the FB itself. In view of the above problems, in this study, an FB structure in a sea lock project was taken as an example. Based on the basic theory of mechanics, the mathematical relationships between the strain in the load-sensitive area of the FB and the mooring force and the mooring angle were quantified, and a dynamic inversion model of the force of a moored ship on an FB is proposed. The accuracy and reliability of the model were verified by data from tests with a physical model of the topside structure of an FB. The results of this research will help to promote the development of intelligent technologies for monitoring and providing early warnings based on the operational state of the FB of a lock, which have important scientific significance and value in how FBs are applied.

## 2. Theoretical Derivation

### 2.1. Basic Assumptions

According to the loading characteristics of the topside structure of an FB, a simplified model was proposed using a statically indeterminate cantilever beam model with a constant cross section considering the linear elastic stage of the structure and material. Moreover, the bottom of the beam model was fixed, and no translation or rotation was allowed at this node. In addition, the boundary constraint of the beam model was hinged at position $L_1$ from the bottom height to constrain the translational displacement of the node in the $X$ and $Y$ directions and allow it to rotate around the $OY$-axis, as shown in Figure 2.

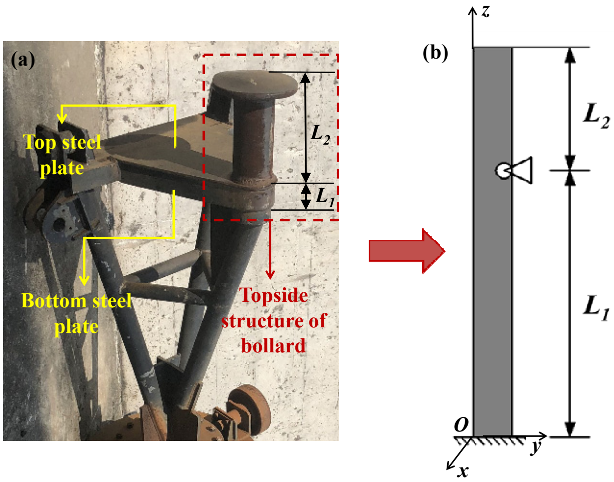


**Figure 2.** The floating bollard (FB) of a ship lock: (**a**) an FB; (**b**) the simplified model of the topside structure of the FB.

For a ship docked in a lock chamber, the mooring angles $\alpha$ (in the horizontal direction) and $\beta$ (in the vertical direction) are defined according to the projection of the mooring line of the FB on the horizontal plane and the vertical plane, respectively, as shown in Figures 3 and 4. When the freeboard height of the ship is higher than the top of the FB, the ship produces an upward mooring force on the bollard, and $\beta > 0$, as shown in Figure 4a. In addition, when the freeboard height is lower than the top of the FB, the ship exerts a downward mooring force on the bollard, i.e., $\beta < 0$, as shown in Figure 4b.

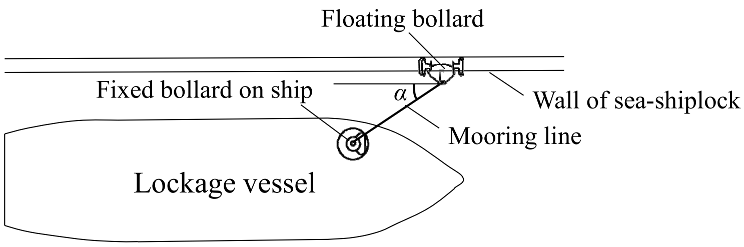


**Figure 3.** Mooring angle $\alpha$ of an FB under the ship mooring force.

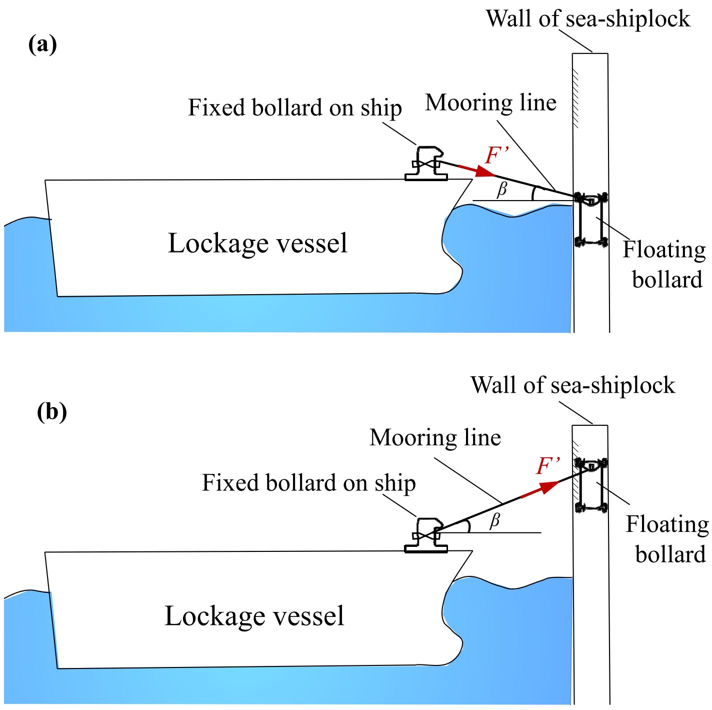


**Figure 4.** Mooring angle $\beta$ of the FB under the ship mooring force: (**a**) $\beta > 0$; (**b**) $\beta < 0$.

*2.2. Mathematical Relationships between the Structural Strain of the FB and Ship Mooring Factors (Force and Angles)*

For any load-sensitive point $P$ on the external surface of the FB topside structure, the strain mainly includes the tensile/compressive strain caused by the axial component $F_z$ and the bending strain caused by the horizontal component $F_{xy}$, as shown in Figure 5.

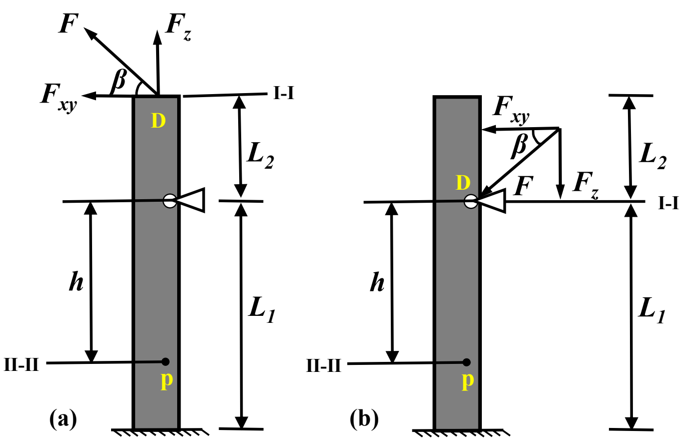


**Figure 5.** Simplified analysis of ship mooring force on the FB: (**a**) $\beta > 0$; (**b**) $\beta < 0$.

2.2.1. When the mooring angle $\beta > 0$

- Tensile strain of the FB topside structure.

When the FB is subjected to the axial component force $F_z$ of the ship mooring force, the axial tensile strain generated by any section at any load-sensitive point $P$ on the topside structure is

$$\begin{cases} F_z = \sigma_1 A_1 \\ \sigma_1 = E_1 \varepsilon_1 \end{cases} \tag{1}$$

It can be deduced that

$$\varepsilon_1 = \frac{F_z}{E_1 A_1} \tag{2}$$

where $F_z$ is the axial component of the ship mooring force; $\varepsilon_1$ is the tensile strain at any load-sensitive point $P$ on the surface of the FB topside structure; and $\sigma_1$ is the tensile stress at any load-sensitive point $P$ on the surface of the FB topside structure. $A_1$ is the cross-sectional area of the FB topside structure and $E_1$ is the elastic modulus of the FB material.

- Bending strain of the FB topside structure.

The section bending moment of the FB topside structure includes $M_{xy}$ and $M_z$, which are generated by the horizontal component of mooring force ($F_{xy}$) and the axial component of mooring force ($F_z$) on any section of the topside structure, respectively.

The $M_{xy}$ generated by the horizontal component $F_{xy}$ on any section of the topside structure can be expressed as

$$M_{xy} = F_{xy} \cdot (2L_1 - 3h) \cdot L_2/2L_1 \tag{3}$$

where $F_{xy}$ is the horizontal component of the ship mooring force; $L_1$ is the length between the fixed support at the bottom of the FB topside structure and the hinged support; $L_2$ is the length of the cantilever section of the FB topside structure; and $h$ is the distance between any load-sensitive point of the bollard body and the hinge supports of the FB topside structure. See Figure 5 for the geometric relationship above.

For the $M_z$ generated by the axial component force $F_z$ on any section of the topside structure, the ship mooring force acts on the topside structure in the form of surface force, and thus

$$M_z = \int_0^{\pi R} \frac{F_z}{\pi R} R \sin\omega dl = \int_0^{\pi} \frac{F_z}{\pi} R \sin\omega d\omega = F_z \cdot (2R/\pi) \tag{4}$$

where $R$ is the ring radius of the axial section of the FB topside structure and $\omega$ is the included angle between any point of the stress surface of the FB topside structure and the connection between the center of the circle and the neutral axis, as shown in Figure 6a.

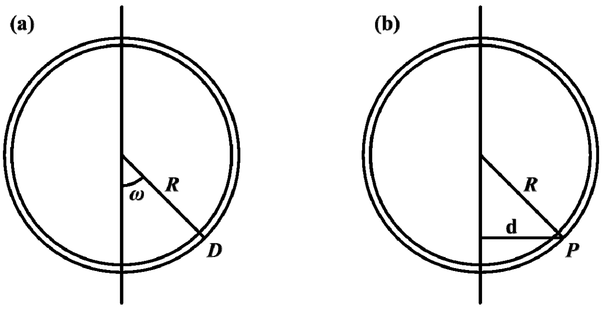


**Figure 6.** Cross sections of the FB: (**a**) section I-I; (**b**) section II-II.

The bending strain at point $P$ on the surface of the FB topside structure can be further deduced:

$$\varepsilon_2 = \frac{M_{xy}}{E_1 I_1} d + \frac{M_z}{E_1 I_1} d \tag{5}$$

where $\varepsilon_2$ is the bending strain at point $P$ on the surface of the FB topside structure; $I_1$ is the moment of inertia of the ring of the topside structure section; and $d$ is the vertical distance between point $P$ on the surface of the topside structure and the neutral axis, as shown in Figure 6b.

By linear superposition of the axial tensile strain $\varepsilon_1$ and the bending strain $\varepsilon_2$, combined with Equations (2)–(5), the actual strain at point $P$ on the surface of the FB topside structure can be derived as follows:

$$\varepsilon = \varepsilon_1 + \varepsilon_2 = \frac{F_z}{E_1 A_1} + \frac{F_{xy}(2L_1 - 3h)L_2/2L_1}{E_1 I_1} d + \frac{F_z(2R/\pi)}{E_1 I_1} d \tag{6}$$

#### 2.2.2. When the Mooring Angle $\beta < 0$

- Compressive strain of the FB topside structure.

When the FB is subjected to the axial component force $F_z$ of the ship mooring force, the axial compressive strain generated by any section corresponding to any load-sensitive point $P$ within the $L_1$ range of the topside structure is

$$\begin{cases} -F_z = \sigma_3 A_1 \\ \sigma_3 = E_1 \varepsilon_3 \end{cases} \tag{7}$$

It can be deduced that

$$\varepsilon_3 = -\frac{F_z}{E_1 A_1} \tag{8}$$

where $\varepsilon_3$ is the compressive strain at any load-sensitive point $P$ on the surface (the following are within the $L_1$ range) of the FB topside structure and $\sigma_3$ is the compressive stress at any load-sensitive point $P$ on the surface of the FB topside structure.

- Bending strain of the FB topside structure.

(1) The $M_{xy}{}'$ generated by the horizontal component of the mooring force $F_{xy}$ on the bollard

When the FB topside structure is subjected to a downward mooring force, the mooring line is directly attached to the fixed steel plate of the FB topside structure, as shown in Figure 2a. The steel plate undergoes tensile deformation due to the horizontal component of the mooring force $F_{xy}$ (see Figure 7). At this time, the deformation ($w$) of the fixed steel plate of the FB topside structure along the $XY$ plane is

$$w = \frac{F_{xy} L_3}{E_2 A_2} \tag{9}$$

where $L_3$ is the length of the steel plate of the FB topside structure; $A_2$ is the cross-sectional area of the steel plate of the FB topside structure; and $E_2$ is the elastic modulus of the steel plate of the FB topside structure.

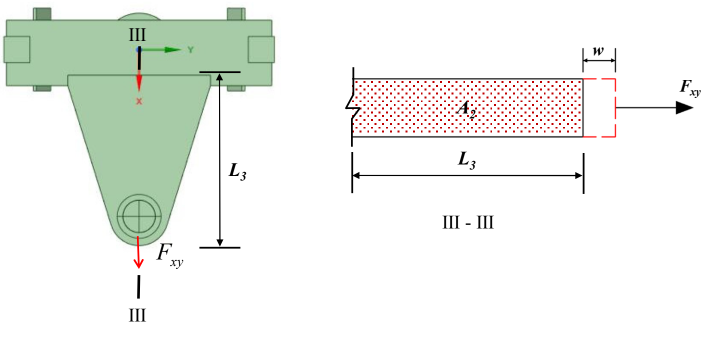


**Figure 7.** Axial deformation of the steel plate on the FB topside structure.

Deformation ($w$) of the steel plate causes bearing displacement of the hinged supports in the simplified model of the bollard when the steel plate of the FB topside structure is deformed in Figure 8.

According to the basic principle of structural mechanics, the reaction force of bearing $D$ can be written as follows:

$$R_D = \frac{3F_{xy} L_3 I_1}{A_2 L_1^3} \tag{10}$$

The $M_{xy}{}'$ of the bollard section is

$$M_{xy}{}' = R_D h = \frac{3F_{xy} L_3 I_1 h}{A_2 L_1^3} \tag{11}$$

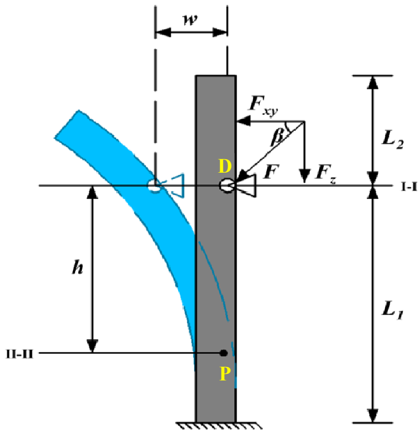


**Figure 8.** Bearing displacement on the hinged supports.

The meanings of the symbols in the formula are the same as above.

(2) The $M_z{}'$ generated by the axial component of mooring force $F_z$ on the bollard

The ship mooring force acts on the F topside structure in the form of surface force, and thus

$$M_z{}' = -M_z = -F_z(2R/\pi) \tag{12}$$

The meanings of the symbols in the formula are the same as above.

The bending strain at point $P$ on the surface of the FB topside structure can be further deduced:

$$\varepsilon_4 = \frac{M_{xy}{}'}{E_1 I_1}d + \frac{M_z{}'}{E_1 I_1}d \tag{13}$$

where $\varepsilon_4$ is the bending strain at point $P$ on the surface of the FB topside structure; the meanings of symbols in the formula are the same as above.

In combination with Equations (8) and (11)–(13), the strain at any load-sensitive point $P$ on the surface of the FB topside structure can be derived as follows:

$$\varepsilon' = \varepsilon_3 + \varepsilon_4 = -\frac{F_z}{E_1 A_1} + \frac{3F_{xy}L_3 h}{A_2 L_1^3 E_1}d - \frac{F_z(2R/\pi)}{E_1 I_1}d \tag{14}$$

*2.3. Mooring Force Dynamic Inversion Model of FBs*

Two strain measurement points ($T$ and $K$) were randomly selected on the surface of the bollard in the $L_1$ range below the steel plate of the FB topside structure, as shown in Figure 9. The distances between the measuring points $T$ and $K$ and the neutral axis were $d_T = R\sin\theta$ and $d_K = R\sin(\theta + \gamma)$, respectively. $R$ was the radius of the axial section ring of the FB; $\theta$ was the angle between point $T$ and the centerline and the neutral axis; and $\gamma$ was the angle between points $T$ and $K$ and the line connecting the center of the circle, as shown in Figure 9. Assuming that the angle between the measuring point $T$ and the gate wall line was $\delta$, the angle (horizontal angle) between the mooring line and the gate wall line was $90° + \theta - \delta$.

Assuming that the total strains at points $T$ and $K$ were $\varepsilon_T$ and $\varepsilon_K$, respectively, according to Equations (6) and (14), we obtained the following:

- When $\beta > 0$,

$$\varepsilon_T = \frac{F_z}{E_1 A_1} + \frac{F_{xy}(2L_1 - 3h)L_2/2L_1}{E_1 I_1}d_T + \frac{F_z(2R/\pi)}{E_1 I_1}d_T \tag{15}$$

$$\varepsilon_K = \frac{F_z}{E_1 A_1} + \frac{F_{xy}(2L_1 - 3h)L_2/2L_1}{E_1 I_1}d_K + \frac{F_z(2R/\pi)}{E_1 I_1}d_K \tag{16}$$

- When $\beta < 0$,

$$\varepsilon_T{}' = -\frac{F_z}{E_1 A_1} + \frac{3F_{xy} L_3 h}{A_2 L_1^3 E_1} d_T - \frac{F_z (2R/\pi)}{E_1 I_1} d_T \tag{17}$$

$$\varepsilon_K{}' = -\frac{F_z}{E_1 A_1} + \frac{3F_{xy} L_3 h}{A_2 L_1^3 E_1} d_K - \frac{F_z (2R/\pi)}{E_1 I_1} d_K \tag{18}$$

where $F_{xy} = F\cos\beta$, $F_z = F\sin\beta$, $d_T = R\sin(\alpha + \delta - 90°)$, and $d_K = R\sin(\alpha + \delta + \gamma - 90°)$.

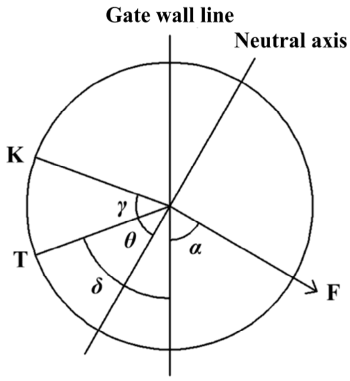


**Figure 9.** Location and geometric angle of the strain-measuring point of the FB.

According to the specification [48] and field measurement statistics [49], the angle between the mooring line and the horizontal plane was taken as $\beta = \pm 15°$, as shown in Figure 4. Therefore, according to Equations (15) and (16) and Equations (17) and (18), when $\beta > 0$ ($\beta = 15°$) and $\beta < 0$ ($\beta = -15°$), the angle $\alpha$ between the mooring line and the wall of the sea lock and the mooring force $F$ acting on the FB topside structure could be obtained. In addition, due to the real-time changes in mooring force $F$ and mooring angle $\alpha$ with time, in Equations (15)–(18) above, $\varepsilon_T = \varepsilon_T(t)$, $\varepsilon_K = \varepsilon_K(t)$, $\varepsilon_T{}' = \varepsilon_T{}'(t)$, and $\varepsilon_K{}' = \varepsilon_K{}'(t)$, as follows:

- When $\beta > 0$ ($\beta = 15°$),

$$\alpha(t) = \arccos\frac{0.259 I_1 [\varepsilon_T(t) - \varepsilon_K(t)]}{A_1 R(m+n)\sqrt{x^2 + y^2}} - \delta - \arctan\frac{y}{x} \tag{19}$$

$$F(t) = \frac{E_1 I_1 [\varepsilon_T(t) - \varepsilon_K(t)]}{R(m+n)[\cos(\alpha+\delta) - \cos(\alpha+\delta+\gamma)]} \tag{20}$$

where $m = 0.966(2L_1 - 3h)L_2/2L_1$, $n = 0.259(2R/\pi)$, $x = \cos\gamma\varepsilon_T(t) - \varepsilon_K(t)$, and $y = \sin\gamma\varepsilon_T(t)$.

- When $\beta < 0$ ($\beta = -15°$),

$$\alpha'(t) = \arcsin\frac{-0.259 A_2 L_1^3 I_1 [\varepsilon_T{}'(t) - \varepsilon_K{}'(t)]}{A_1 \cdot R \cdot (m' - n')\sqrt{(x')^2 + (y')^2}} - \delta - \arctan\frac{y'}{x'} \tag{21}$$

$$F'(t) = \frac{A_2 L_1^3 E_1 I_1 [\varepsilon_T{}'(t) - \varepsilon_K{}'(t)]}{R(m' - n')[\cos(\alpha+\delta) - \cos(\alpha+\delta+\gamma)]} \tag{22}$$

where $m' = 2.898hL_3I_1$, $n' = -0.259A_2{L_1}^3(2R/\pi)$, $x' = \sin\gamma\varepsilon_T{}'(t)$, and $y' = \varepsilon_K{}'(t) - \cos\gamma\varepsilon_T{}'(t)$.

In summary, under the condition that the distance $h$ between the position of the mooring line and the cross section of any load-sensitive point on the surface of the FB and the vertical angle $\beta$ were known, the strain data information of any load-sensitive point on the surface of the FB were measured in real time, and the ship mooring factor acting on the FB topside structure was obtained by combining the dynamic inversions of Equations (19) and (20) and Equations (21) and (22), including the mooring force $F$ and mooring angle $\alpha$.

## 3. Model Validation by Tests of a Structural Physical Model

A test was conducted on a physical model of the FB topside structure under the mooring force, and strain data at two points ($T$ and $K$) of the FB topside structure under the different mooring forces and mooring angles were obtained and substituted into Equations (19)–(22) to obtain the values of the mooring force and mooring angle predicted by the model. The accuracy of the dynamic inversion model of the mooring force of the FB was verified by comparing the values of mooring force and mooring angle predicted by the model with the standard values for experimental loading.

### *3.1. Physical Model Test of the Floating Bollard Topside Structure*

#### 3.1.1. Design of the Physical Model for the Floating Bollard Topside Structure

According to the structural type and simplified model of the FB in Figure 2, considering the constraints of the top and bottom steel plates under the mooring force, a physical model of the upper part of the FB topside structure with a model scale of 1:1 was established (see Figure 10a). Q235B steel was used as the raw material of the FB topside structure. The boundary conditions of the FB topside structure were simulated by fixing the top and bottom steel plates with M24 high-strength anchor bolts with a strength grade of C30 on the concrete dolphin.

The physical model is shown in Figure 10b.

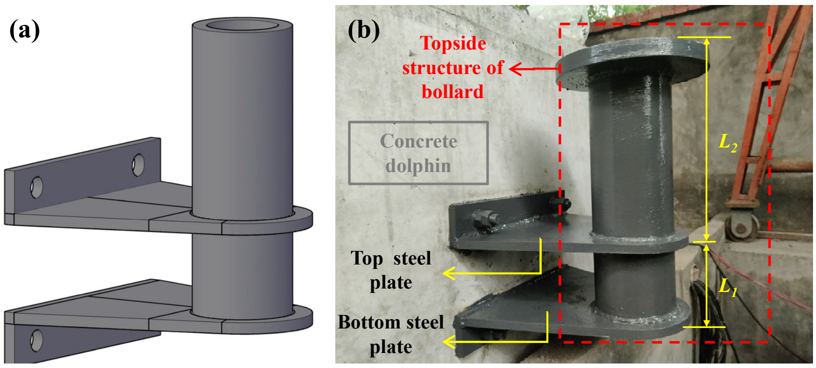


**Figure 10.** Test of the physical model of the topside structure of the floating bollard: (**a**) model design; (**b**) physical model.

#### 3.1.2. Test Program of the Physical Model

- Instruments and equipment.

(1) Loading equipment and device for simulating ship mooring force

The ship mooring force was simulated by the tension on the winch installed on the gantry crane in this experiment, and the physical model of the FB topside structure was then loaded. The most appropriate loading mode was realized by moving the winch along the horizontal direction to the left and right, and the maximum loading capacity was 3 t, as shown in Figure 11.

To more accurately simulate the change in mooring angle in the test of the physical model, top and bottom devices were added between the mooring force loading device and the physical model of the FB topside structure to simulate the two loading modes when the mooring angle $\beta$ was $\pm 15°$. In addition, the change in the horizontal angle $\alpha$ of the mooring force of the ship from 35° to 145° was realized by adding a limit hook on the device. A schematic figure of the device is shown in Figures 12 and 13a.

(2) Measuring equipment for ship mooring force

The load imposed on the mooring line by the ship mooring force simulation loading device was measured by a tensiometer installed on the mooring line, as shown in Figure 13b.

(3) Dynamic strain data acquisition equipment for the $K$ and $T$ measuring points of the FB topside structure

The dynamic strain data acquisition equipment mainly included a DH1101 welded strain gauge and a DH2004 wireless distributed monitor. The DH2004 wireless distributed monitor was composed of a dynamic strain data collector, controller, acquisition software, signal display screen, and other parts, as shown in Figure 13c.


**Figure 11.** Device for modelling the ship mooring force: (**a**) overall structure of the device; (**b**) winch; (**c**) drag hook.

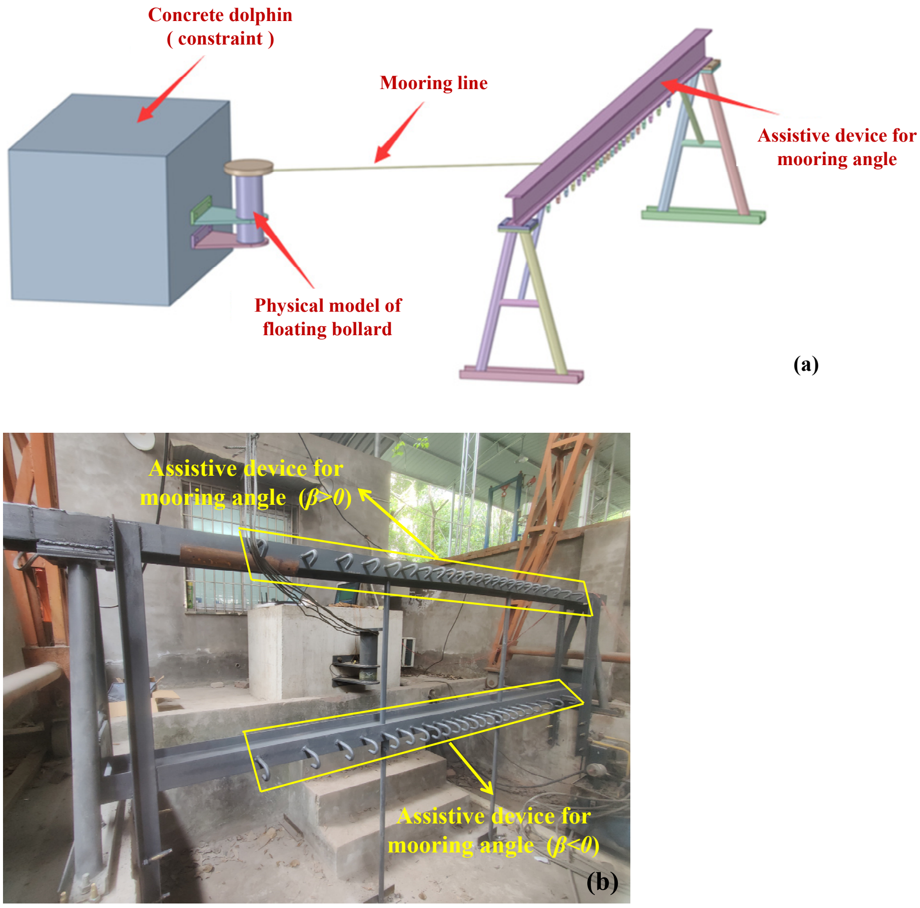


**Figure 12.** Device for the ship mooring angle: (**a**) schematic design; (**b**) schematic diagram of the device.

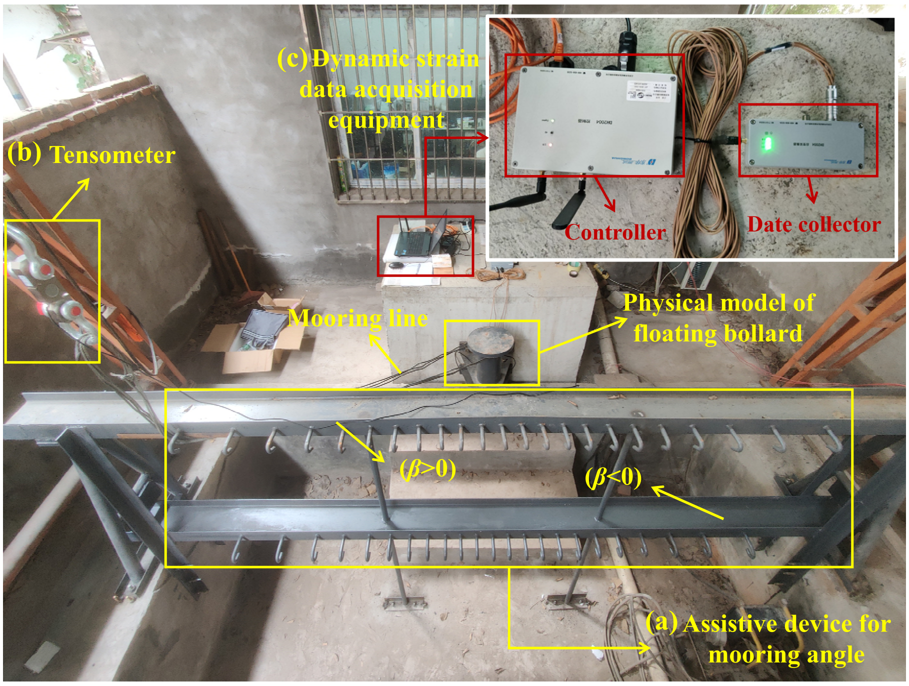


**Figure 13.** Test of the physical model of the FB topside structure.

- Location of the strain measuring points.

According to the geometric size of the physical model of the FB topside structure, points $T$ and $K$ were 112 mm above the bottom steel plate. The angle between the two measurement points of $T$ and $K$ and the centerline was $\gamma$ = 20°, and the angle between point $T$ and the line of the lock wall was $\delta$ = 80°, as shown in Figure 14a–c. The DH1101 welded strain gauge was installed at the above $T$ and $K$ points and was waterproof and moistureproof, as shown in Figure 14d.

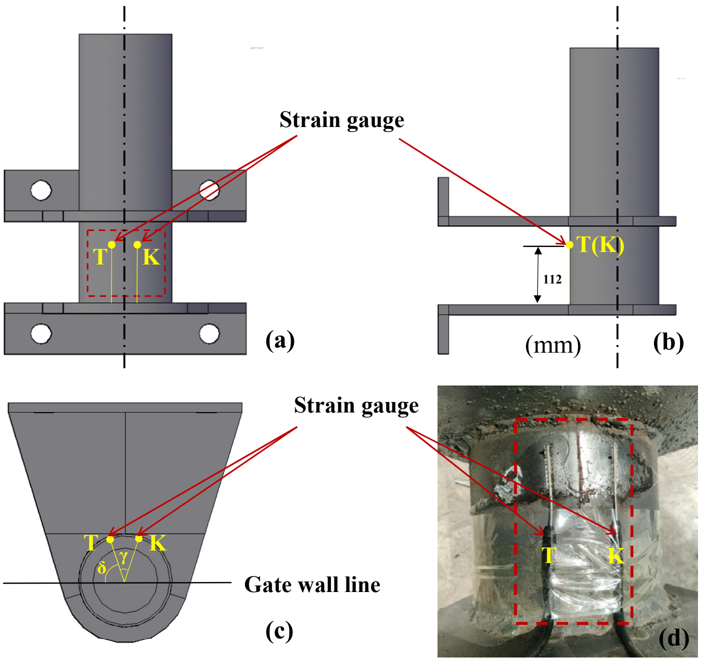


**Figure 14.** Positions of the strain gauges: (**a**) front view; (**b**) side view; (**c**) top view; (**d**) schematic of the positions.

## 3.2. Results and Discussion

Through the physical model test of the upper part of the FB topside structure, strain data of the $T$ and $K$ points of the FB topside structure under the different standard values of mooring force and mooring angle were obtained, and they were substituted into the dynamic inversion model in Equations (19)–(22) to predict the values for mooring force and mooring angle. The rationality and reliability of the dynamic inversion model of FB mooring force were verified by comparing the predictions of the model with standard mooring force and mooring angle values.

### 3.2.1. Test Results for Mooring Force

The change in mooring force $F$ with increasing horizontal angle $\alpha$ when $\beta = \pm 15°$ was simulated in the test of the physical model, and the measured results are shown in Figure 15.

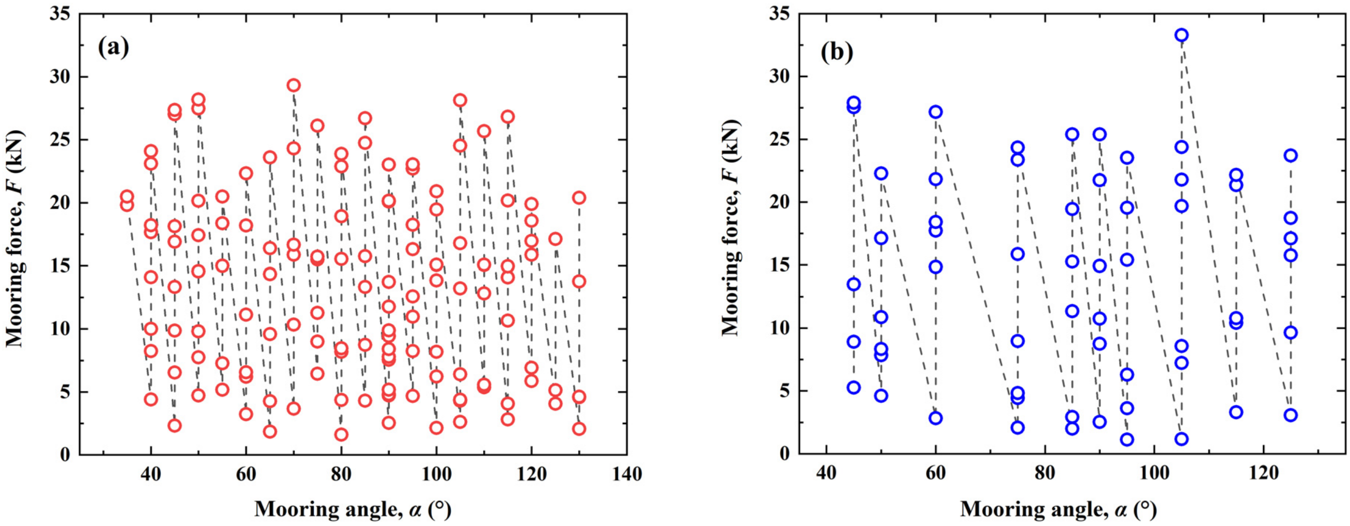


**Figure 15.** Test results for mooring force: (**a**) $\beta = 15°$ ($\beta > 0$); (**b**)$\beta = -15°$ ($\beta < 0$).

### 3.2.2. Test Results of Strain

According to Figure 15, strain data at the two measuring points $T$ and $K$ of the FB topside structure were obtained under the loading conditions of different mooring forces ($F$) and horizontal angles ($\alpha$) when $\beta = \pm 15°$, as shown in Figure 16.

### 3.2.3. Variation in Strain at Points $T$ and $K$ with Increasing Mooring Force

The changes in strain at points $T$ and $K$ of the FB topside structure with increasing mooring forces under different horizontal mooring angles ($\alpha$) are shown in Figure 17. The standard values of $\alpha = 115°$, 90°, and 60° were used as representatives, and the variation of strain at points $T$ and $K$ on the surface of the FB topside structure was analyzed.

As shown in Figure 17, the strains at points $T$ and $K$ of the FB topside structure showed a nearly linear trend with increasing mooring force ($F$), and the trends remained consistent for different horizontal mooring angles ($\alpha$) and vertical mooring angles ($\beta$). The strains at the load-sensitive points of the FB topside structure were more affected by mooring angle $\alpha$ when $\beta > 0$. On the surface of the FB topside structure, the strain at measuring point $T$ reached a maximum at $\alpha = 115°$, and the strain at measuring point $K$ reached a maximum at $\alpha = 90°$.

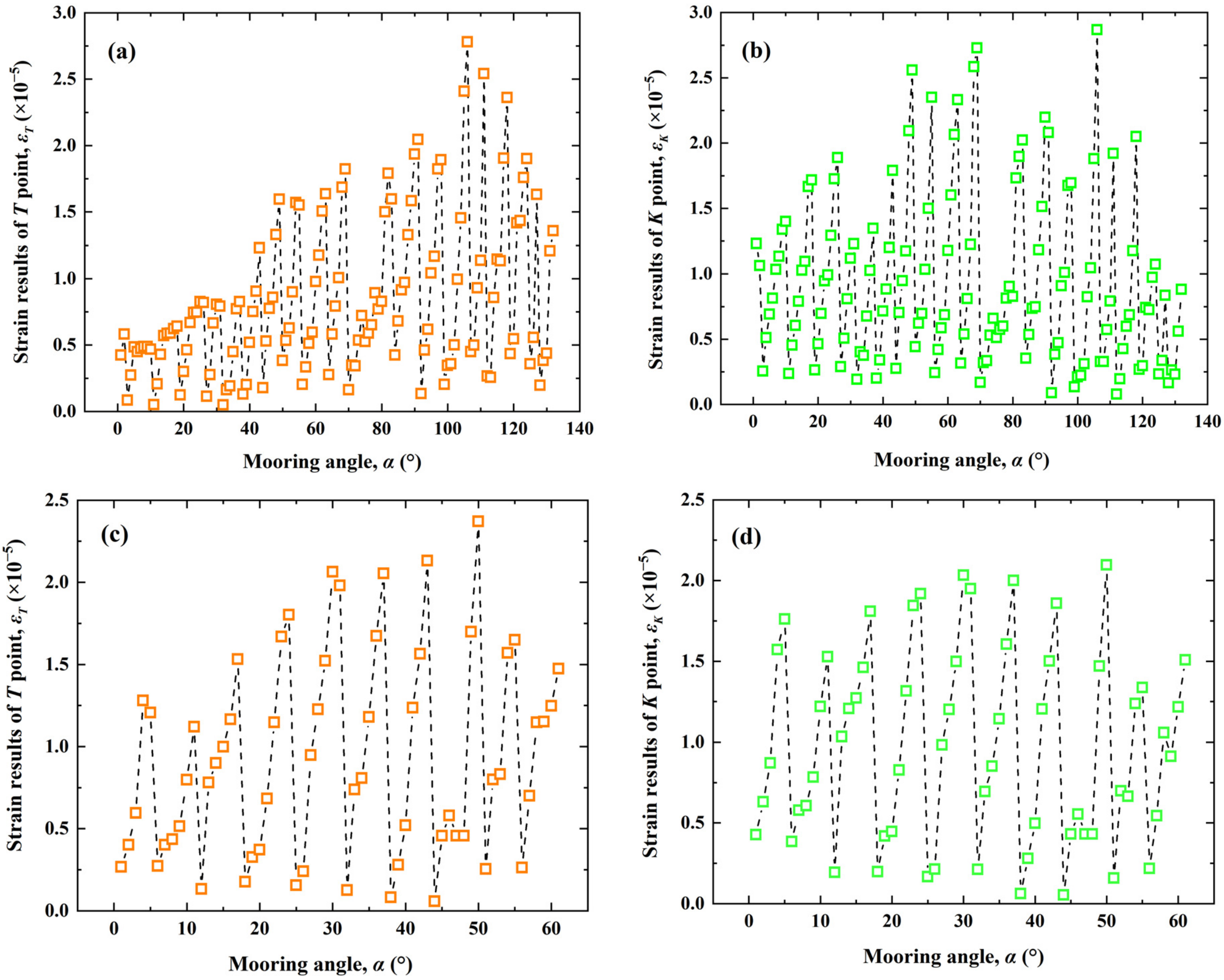


**Figure 16.** Test results for strain: (**a**) strain at point $T$ when $\beta > 0$; (**b**) strain at point $K$ when $\beta > 0$; (**c**) strain at point $T$ when $\beta < 0$; (**d**) strain at point $K$ when $\beta < 0$.

### 3.2.4. Verification of Mooring Force from the Dynamic Inversion Model for the FB of the Sea Lock

To quantitatively estimate the differences between the predictions of the dynamic inversion model and the results of the test of the physical model, the relative errors of mooring angle $\alpha$ and mooring force $F$ when $\beta = \pm 15°$ were calculated, as shown in Figures 18 and 19. The figures show that the relative errors between the predictions of the dynamic inversion model proposed in this paper and the measured standard values for the physical model of the FB topside structure were less than 20%, and the error of mooring angle $\alpha$ was within the range of $\pm 15\%$, which verified the accuracy and reliability of the model.

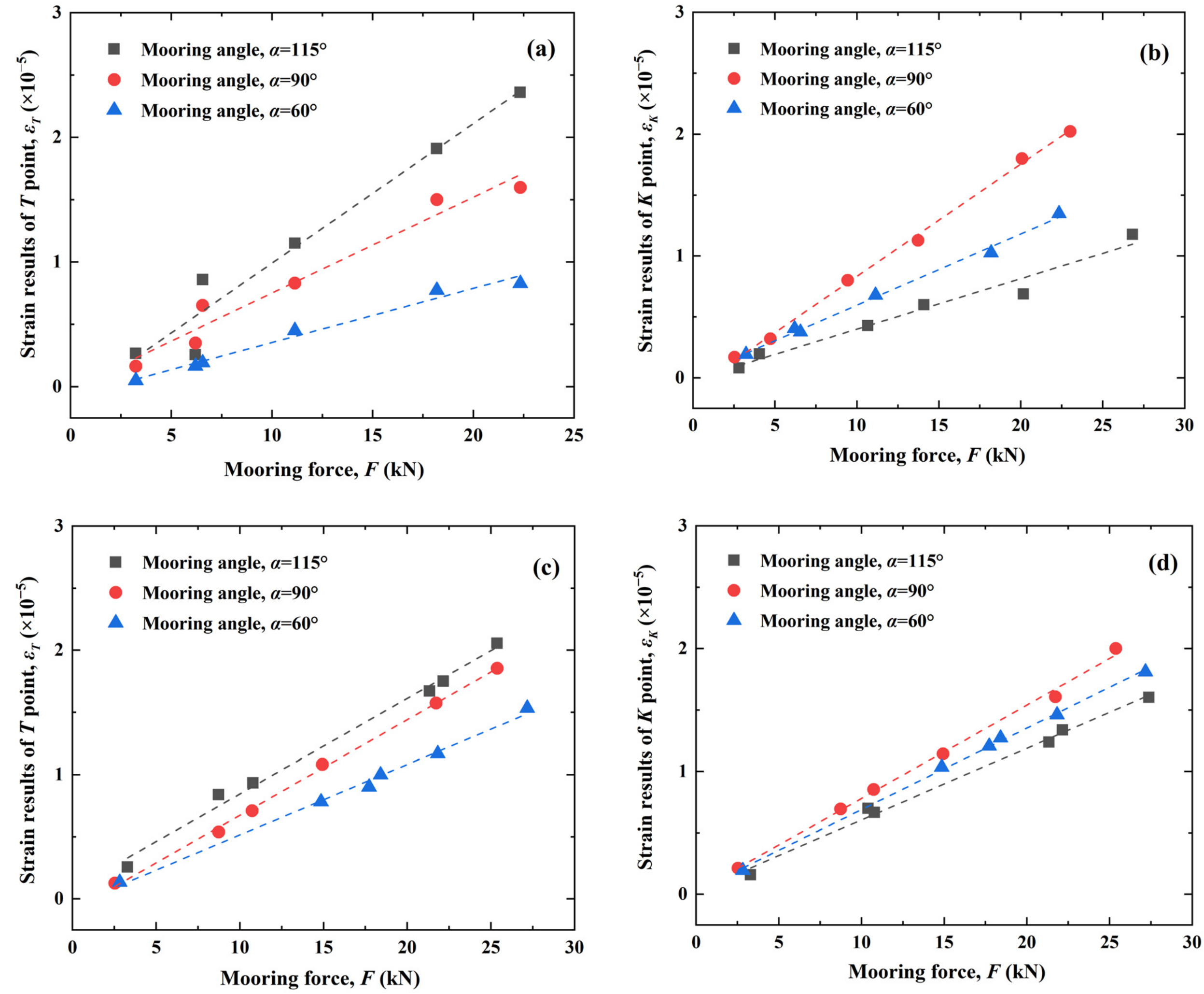


**Figure 17.** Strain variation with mooring force: (**a**) strain variation at point $T$ when $\beta > 0$; (**b**) strain variation at point $K$ when $\beta > 0$; (**c**) strain variation at point $T$ when $\beta < 0$; (**d**) strain variation at point $K$ when $\beta < 0$.

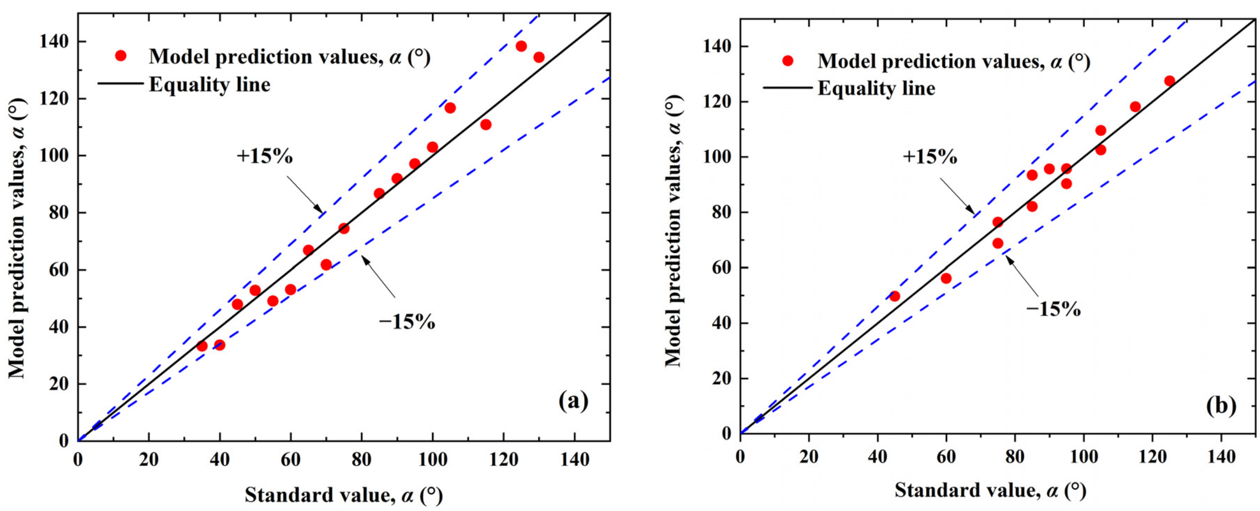


**Figure 18.** Calculated errors of mooring angle $\alpha$: (**a**) $\beta > 0$; (**b**) $\beta < 0$.

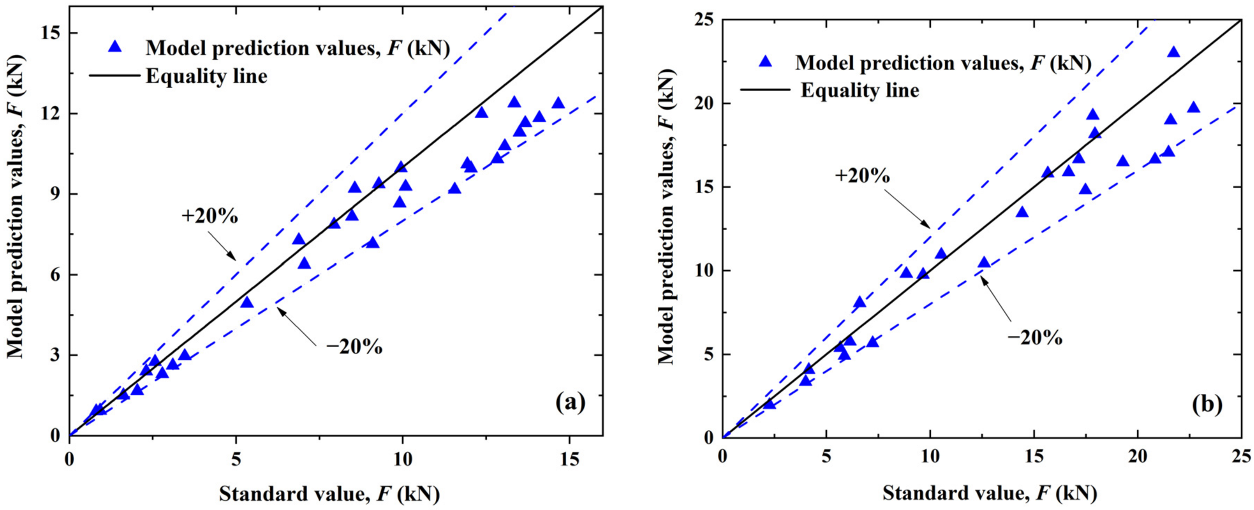


**Figure 19.** Calculated errors of mooring force $F$: (**a**) $\beta > 0$; (**b**) $\beta < 0$.

## 4. Discussion and Conclusions

In response to the safety of ship mooring and the safe operation of FBs in sea locks, and taking the structure of the FB in a sea lock project as an example, research was conducted on methods to obtain important mooring factors such as the mooring force and mooring angle of the FB. According to the basic theory of mechanics, the mathematical relationships between the structural strain at the load-sensitive points of the FB topside structure and the mooring force and angle were quantified, and a dynamic inversion model of ship mooring force was established with an FB as the main object. On this basis, the accuracy of the model was verified by comparing the predictions of the model with data from tests of a physical model of the FB topside structure. Real-time feedback from the strain signal of the FB structure to mooring force information can be realized by applying this model, which is helpful to dynamically perceive the mooring force acting on the FB and avoid the occurrence of safety accidents in sea locks. The specific research conclusions are as follows:

(1) The FB topside structure was simplified as a model of a statically indeterminate linearly elastic cantilever beam with a constant cross section, and a dynamic inversion model was established to reflect the quantitative relationships between the strain at the load-sensitive measuring points of the FB structure and the mooring factors of the ship (mooring force, mooring angle). The proposed model could quickly and efficiently be inverted to obtain important information such as the mooring force and mooring angle acting on the topside structure of the FB.

(2) A test of a physical model of the FB topside structure was conducted under mooring force. According to the test data, the measured results for the FB structural strain under different mooring angles increased gradually with increasing mooring force, which was consistent with the actual situation.

(3) The maximum relative error between the mooring force and mooring angle calculated by the dynamic inversion model and the measured results of the physical model test was only 20%, and the accuracy and reliability of the dynamic inversion model of the mooring force on the FB of the sea lock were verified.

Traditional monitoring methods cannot effectively reflect the stress characteristics of the FB structure itself. Tracking and monitoring of the safety state of the mooring in the lock chamber of the navigation ship cannot be fully covered in real time, and it is difficult to realize early warning systems and post-accountability for safety accidents in sea locks. The dynamic inversion model of ship mooring force proposed in this paper with an FB as the main object can realize real-time feedback from the strain signal of the load-sensitive area of the FB structure to mooring force information and effectively improve the ability of the navigation hub management unit to evaluate the safety status of ship mooring and the safety of the FB. In the future, a series of studies will be carried out, including research related to an online long-term active intelligent monitoring method and an intelligent monitoring system for FBs at sea locks. It is possible to apply the demonstration in actual sea lock engineering so as to realize the construction of a digital perception and supervision network for FBs at sea locks, thus guaranteeing the intelligent operation and maintenance of FBs at sea locks.

**Author Contributions:** Conceptualization, formal analysis, methodology: L.W.; investigation, data curation, writing—original draft: Z.X.; validation: D.S.; supervision, resources: M.L.(Mingwei Liu); writing—review and editing: J.Y.; visualization, data curation: M.L. (Minglong Li) All authors have read and agreed to the published version of the manuscript.

**Funding:** This research was funded by the Science & technology Innovation Project of Chongqing Education Commission (KJCX2020030), the Key Project of Technology Innovation and Application Development in Chongqing of China (CSTB2022TIAD-KPX0097), the Talents Plan Project in Chongqing of China (cstc2021ycjh-bgzxm0053), the National Natural Science Foundations of China (52279124, 52209156), and the Research and Innovation Program for Graduate Students in Chongqing Jiaotong University (2023S0042).

**Institutional Review Board Statement:** Not applicable.

**Informed Consent Statement:** Not applicable.

**Data Availability Statement:** Data are contained within the article.

**Conflicts of Interest:** The authors declare no conflict of interest.

## Abbreviations

**List of symbols**

| | | | |
|---|---|---|---|
| $A_1$, $A_2$ | Cross-sectional area of the bollard and the steel plate | $R$ | Ring radius of the axial section of the FB topside structure |
| $d$ | Vertical distance from the strain measuring point to the neutral axis | $R_\mathrm{D}$ | Reaction force of bearing $D$ |
| $d_T$, $d_K$ | Distance of the strain measuring points $T$ and $K$ from the neutral axis | $\varepsilon_1$, $\varepsilon_3$ | Tensile strain and compressive strain of the FB topside structure: $\beta > 0$, $\beta < 0$ |
| $E_1$, $E_2$ | Elastic modulus of the bollard and the steel plate | $\varepsilon_2$, $\varepsilon_4$ | Bending strain of the FB topside structure: $\beta > 0$, $\beta < 0$ |
| $F$ | Mooring force | $\varepsilon$, $\varepsilon'$ | Actual strain of the FB topside structure: $\beta > 0$, $\beta < 0$ |
| $F_z$,$F_{xy}$ | Axial component and horizontal component of mooring force | $\sigma_1$, $\sigma_3$ | Tensile stress and compressive stress of the FB topside structure: $\beta > 0$, $\beta < 0$ |
| $h$ | Distance between any load-sensitive point of the bollard and hinge supports on the FB topside structure | $\omega$ | The included angle between any point of the stress surface of the FB topside structure and the connection between the center of the circle and the neutral axis |
| $I_1$ | Inertia moment of a ring of the bollard section | $\theta$ | The angle between the line connecting the measuring point T and the center of the circle and the neutral axis |
| $L_1$ | Length of the FB between the fixed support and hinged support | $\gamma$ | The angle between the $T$ and $K$ measuring points and the center of the circle |
| $L_2$ | Length of the cantilever section of the FB | $\delta$ | The angle between measuring point $T$ and the circle center line and the gate wall line |
| $L_3$ | Length of the steel plate | $w$ | Deformation of the steel plate |
| $M_z$, $M_{xy}$; $M_z'$, $M_{xy}'$ | Axial component and horizontal component of the section bending moment: $\beta > 0$, $\beta < 0$ | $\alpha$, $\beta$ | Mooring angles in the horizontal direction and vertical direction |

## References


1. Calvo Gobbetti, L.E. Design of the filling and emptying system of the new Panama Canal locks. *J. Appl. Water Eng. Res.* **2013**, *1*, 28–38. [CrossRef]
2. Yang, Y.; Cao, Y.; Yang, L.; Li, Z. Hydraulics analysis of filling and emptying system for evaluating the impact of water level variation on downstream of ship locks. *Adv. Water Sci.* **2017**, *28*, 76–85. [CrossRef]
3. Costas, R.; Figuero, A.; Peña, E.; Sande, J.; Rosa-Santos, P. Integrated approach to assess resonance between basin eigenmodes and moored ship motions with wavelet transform analysis and proposal of operational thresholds. *Ocean Eng.* **2022**, *247*, 110678. [CrossRef]
4. Liu, C.; Qi, J.; Chu, X.; Zheng, M.; He, W. Cooperative ship formation system and control methods in the ship lock waterway. *Ocean Eng.* **2021**, *226*, 108826. [CrossRef]
5. Lone, E.N.; Sauder, T.; Larsen, K.; Leira, B.J. Fatigue reliability of mooring chains, including mean load and corrosion effects. *Ocean Eng.* **2022**, *266*, 112621. [CrossRef]
6. Rosa-Santos, P.; Taveira-Pinto, F.; Veloso-Gomes, F. Experimental evaluation of the tension mooring effect on the response of moored ships. *Coast. Eng.* **2014**, *85*, 60–71. [CrossRef]
7. Yang, Y.; Yuan, X.; Li, Y.; He, Z.; Zhang, S.; Zheng, S. Effect of time-varying corrosion on the low-cycle fatigue mechanical properties of wire rope. *Ocean Eng.* **2022**, *250*, 111027. [CrossRef]
8. Yang, Y.; Zhang, X.; He, Z.; Guo, J.; Liu, Y. Uniaxial behaviour and corrosion-welding-based constitutive model of marine structural steel. *Ocean Eng.* **2021**, *235*, 109370. [CrossRef]
9. Fan, T.; Qiao, D.; Yan, J.; Chen, C.; Ou, J. An improved quasi-static model for mooring-induced damping estimation using in the truncation design of mooring system. *Ocean Eng.* **2017**, *136*, 322–329. [CrossRef]
10. Lian, Y.; Liu, H.; Yim, S.C.; Zheng, J.; Xu, P. An investigation on internal damping behavior of fiber rope. *Ocean Eng.* **2019**, *182*, 512–526. [CrossRef]
11. Xiong, L.; Yang, J.; Zhao, W. Dynamics of a taut mooring line accounting for the embedded anchor chains. *Ocean Eng.* **2016**, *121*, 403–413. [CrossRef]
12. Cheng, X.; Li, S.; Wang, G. Experimental Study on Hydrodynamic Characteristics of Barge-Type Breakwaters under Different Mooring Methods. *J. Mar. Sci. Eng.* **2023**, *11*, 1016. [CrossRef]
13. Jha, A.; Subedi, D.; Lovsland, P.O.; Tyapin, I.; Cenkeramaddi, L.R.; Lozano, B.; Hovland, G. Autonomous Mooring towards Autonomous Maritime Navigation and Offshore Operations. In Proceedings of the 2020 15th IEEE Conference on Industrial Electronics and Applications (ICIEA 2020), Kristiansand, Norway, 9–13 November 2020; IEEE: Piscataway, NJ, USA, 2020; pp. 1171–1175.
14. Thorenz, C.; Bousmar, D.; Dubbelman, J.; Jun, L.; Spitzer, D.; Veldman, J.; Augustijn, J.R.; Kortlever, W.; Hartley, A.; Moreno, A.; et al. PIANC Working Group 155 "Ship Behaviour in Locks and Lock Approaches". In Proceedings of the 33rd PIANC World Congress, San Francisco, CA, USA, 1–5 June 2014.
15. Heitmann, C.; Weber, D.; Dlugosch, J.; Feindt, F.; Pollmann, J.; Roller, D. The mooring program for the port of Hamburg. *Bautechnik* **2022**, *99*, 384–395. [CrossRef]
16. Yu, n.; Kim, S.-Y.; Lee, Y.-S. A Study on the Evaluation of Safety Stiffness from Ship's Mooring Bollards. *J. Korean Navig. Port Res.* **2019**, *43*, 9–15. [CrossRef]
17. Andrade, N.R.C.; Tavares, F.; Pérez, R.; Baz, M. Concrete durability of the new Panama Canal: Background and aspects of testing. In *Marine Concrete Structures*; Elsevier: Amsterdam, The Netherlands, 2016; pp. 429–458. [CrossRef]
18. Wijsman, J.W.M. *Panama Canal Extension: A Review on Salt Intrusion into Gatun Lake*; Report Number C215/13; IMARES: Yerseke, The Netherlands, 2011.
19. Ning, W. Discussion on the construction concept and scheme of Pinglu Canal. *Hydro-Sci. Eng.* **2022**, *3*, 1–8. [CrossRef]
20. Chen, C.; Li, Y. Real-time tracking and dynamic berthing information extraction system with 2D LiDAR data. *Ocean Eng.* **2023**, *276*, 114181. [CrossRef]
21. Hao, Q.; Zhang, J.; Zhu, X.; Liu, J. Responses of Large-ship Mooring Forces Based on Actual Measurement. *J. Ship Mech.* **2021**, *25*, 1685–1698. [CrossRef]
22. Katsoudas, A.S.; Silionis, N.E.; Anyfantis, K.N. Structural health monitoring for corrosion induced thickness loss in marine plates subjected to random loads. *Ocean Eng.* **2023**, *273*, 114037. [CrossRef]
23. Kim, S. A Study on Analysis of Mooring Safety Sensitivity According to the Arrangement of Bitt Against Gust. *J. Korean Soc. Mar. Environ. Saf.* **2020**, *26*, 767–776. [CrossRef]
24. Lee, K.-H.; Han, H.-S.; Park, S. Failure analysis of naval vessel's mooring system and suggestion of reducing mooring line tension under ocean wave excitation. *Eng. Fail. Anal.* **2015**, *57*, 296–309. [CrossRef]
25. Sáenz, S.S.; Diaz-Hernandez, G.; Schweter, L.; Nordbeck, P. Analysis of the Mooring Effects of Future Ultra-Large Container Vessels (ULCV) on Port Infrastructures. *J. Mar. Sci. Eng.* **2023**, *11*, 856. [CrossRef]
26. Ding, S.X.; Zhao, T.S.; Gao, F.; Tang, Z.F.; Jin, B.Q. Research on a motion-inhibition fuzzy control method for moored ship with multi-robot system. *Ocean Eng.* **2022**, *248*, 110795. [CrossRef]
27. Wang, J.; Gong, J. Mooring force calculation of flexible berthed structures. *Hydro-Sci. Eng.* **2010**, *31*, 107–113. [CrossRef]
28. Wang, J.; Noh, J. Calculating the Mooring Force of a Large LNG Ship based on OCIMF Mooring Equipment Guidelines. *J. Korean Soc. Mar. Environ. Saf.* **2022**, *28*, 594–600. [CrossRef]

29. De Carvalho, A.v.L.B.; Campello, E.M.B.; Franzini, G.R.; Skaf, K.J. An assessment of mooring systems' forces of ships berthed at dolphins. *Ocean Eng.* **2022**, *253*, 111090. [CrossRef]
30. Sundar, V.; Sundaravadivelu, R.; Kalyani, M. Forces due to oblique waves on a submerged open moored cylinder in deep waters. *Ocean Eng.* **2005**, *32*, 651–666. [CrossRef]
31. Wu, L.; Wu, B.; Shu, D.; Liu, B.; Li, Y. Study of evaluation methods of ship mooring force in stationary berth of open sea. *J. Waterw. Harb.* **2014**, *35*, 489–496.
32. Wu, J.; Shu, Y.; Zhou, S.; Bai, L.; Cao, S. Structure monitoring mothod and experiment of large-scale wharf bollards. *Opt. Precis. Eng.* **2021**, *29*, 1631–1639. [CrossRef]
33. Cho, S.R.; Choung, J.; Oh, C.M.; Lee, K.S.; Kim, J.Y. Ultimate load capacities of mooring bollards and hull foundation structures. *Ocean Eng.* **2010**, *37*, 770–776. [CrossRef]
34. Onishchenko, D.A.; Marchenko, A.V. Modelling of the passive turning of a turret moored vessel in conditions of compact ice. *Appl. Ocean Res.* **2019**, *90*, 101837. [CrossRef]
35. Van Zwijnsvoorde, T.; Vantorre, M.; Eloot, K.; Ides, S. Safety of container ship (un)loading operations in the Port of Antwerp Impact of passing shipping traffic. *Marit. Bus. Rev.* **2019**, *4*, 106–127. [CrossRef]
36. Xiong, L.; Lu, H.; Yang, J.; Zhao, W. Motion responses of a moored barge in shallow water. *Ocean Eng.* **2015**, *97*, 207–217. [CrossRef]
37. De Mulder, T.; Verelst, K.; Vercruysse, J.; De Cock, W.; Haegeman, M. On hawser force criteria for navigation lock design: Case study of maritime locks in port of Antwerp. In Proceedings of the 32nd PIANC Congress, 125th Anniversary PIANC—Setting the Course, Liverpool, UK, 10–14 May 2010.
38. Nogueira, H.I.S.; Ven, P.v.d.; O'Mahoney, T.; Loor, A.D.; Kortlever, W. Effect of Density Differences on the Forces Acting on a Moored Vessel While Operating Navigation Locks. *J. Hydraul. Eng.* **2018**, *144*, 1445. [CrossRef]
39. De Mulder, T. Mooring forces and ship behaviour in navigation locks. *Innov. Navig. Lock Des.* **2009**, *15*, 17.
40. Ma, X.; Hu, Y.; Li, Z. Impact of an energy dissipator on mooring conditions in ultra-high head locks with a comprehensive uniform-strength evaluation. *Ocean Eng.* **2022**, *266*, 112806. [CrossRef]
41. Sun, L.; Li, H.; Du, Y. Research on dynamic tension Measurement technology of Floating mooring bollards of shipLocks. *China Water Transp.* **2022**, *22*, 67–69+109.
42. Qiao, D.; Yan, J.; Liang, H.; Ning, D.; Li, B.; Ou, J. Analysis on snap load characteristics of mooring line in slack-taut process. *Ocean Eng.* **2020**, *196*, 106807. [CrossRef]
43. Huang, W.; Liu, H.; Lian, Y.; Li, L. Modeling nonlinear time-dependent behaviors of synthetic fiber ropes under cyclic loading. *Ocean Eng.* **2015**, *109*, 207–216. [CrossRef]
44. Lian, Y.; Liu, H.; Zhang, Y.; Li, L. An experimental investigation on fatigue behaviors of HMPE ropes. *Ocean Eng.* **2017**, *139*, 237–249. [CrossRef]
45. Liu, M.; Zeng, L.; Qi, J.; Jiang, T. Numerical simulation of stress state of floating bollards of ship lock. *Port Waterw. Eng.* **2020**, *12*, 112–117. [CrossRef]
46. Liu, M.; Li, M.; Wu, L.; Jiang, T.; Zhao, D. Mechanical Model of Load-Bearing Response of Floating Bollard of Ship Lock. *J. Choncqing Jiaotong Univ. Nat. Sci.* **2022**, *41*, 127–132. [CrossRef]
47. Liu, M.; Wang, Z.; Wu, L.; Li, M.; Yang, J. Safety monitoring method for mooring lines of floating bollards in ship lock. *Port Waterw. Eng.* **2023**, *3*, 85–91. [CrossRef]
48. Technical Management Office of Water Transport Planning and Design Institute. General design specification for mooring post members. *Port Waterw. Eng.* **1978**, 3–17.
49. Chen, Z. Research on Large-scale Ship Parameters Based on Mooring Safety in Three Gorges Ship Lock. Masters Thesis, Wuhan University of Technology, Wuhan, China, 2017.